KFUPM
Journal of Undergraduate Research International

Diamond Open Access 9

Article Bioengineering

Effect of Zn^{2+} and Cd^{2+} Incorporation into Mg-MOF-74 on Antibacterial Activity Against *Escherichia coli*

Omar Buqes, Amjad Khalil* and Aasif Helal

Cite https://doi.org/10.64589/juri/231585

Submitted: March 31, 2026 **Revised:** May 11, 2026 **Accepted:** May 13, 2026

ABSTRACT

Metal-organic frameworks (MOFs) have attracted increasing research interest as antibacterial materials because their compositions can be modified via metal incorporation, thus offering a potential strategy for developing alternatives to conventional antimicrobial agents in the context of antimicrobial resistance (AMR). In this study, MOF-74 was used as a shared parent framework to compare the effects of Zn^{2+} and Cd^{2+} incorporation into Mg-MOF-74 on its antibacterial activity against *Escherichia coli*. Three related MOF-74 variants, Mg-MOF-74, Zn-Mg-MOF-74, and Cd-Mg-MOF-74, which share the same crystal structure and organic linker were evaluated using a broth-based OD_{600} growth inhibition assay over 24 h at concentrations of 0-2.22 mg/mL. This allows the effects of metal addition on antibacterial performance to be isolated and compared directly under identical structural and experimental conditions. All three MOF materials showed concentration-dependent inhibition of bacterial growth. At 0.11 mg/mL, Zn-Mg-MOF-74 showed the strongest early inhibition (GI% = 16.4%), followed by Cd-Mg-MOF-74 (GI% = 11.1%), whereas Mg-MOF-74 showed limited inhibition (GI% = 3.9%). This result indicates that incorporation of Zn^{2+} or Cd^{2+} improved the antibacterial performance of the MOF relative to the Mg-only framework, particularly at low concentrations. At 2.22 mg/mL, Zn-Mg-MOF-74 produced the greatest terminal inhibition (OD_{600} = 0.0955, GI% = 88.1%), followed by Cd-Mg-MOF-74 (OD_{600} = 0.1169, GI% = 85.5%) and Mg-MOF-74 (OD_{600} = 0.1394, GI% = 83.9%). Overall, these findings demonstrate that metal-node composition influences antibacterial performance of the MOF-74 system and supports the use of Zn-incorporated and Cd-incorporated Mg-MOF-74 as tunable platforms for the rational design of bimetallic MOF-based antibacterial materials.

Keywords: metal-organic frameworks, MOF-74, bimetallic materials, antibacterial activity, antimicrobial resistance, *Escherichia coli*, zinc, cadmium

1. INTRODUCTION

Bacterial infectious diseases remain a leading cause of morbidity and mortality worldwide, a burden strongly shaped by the emergence and spread of antimicrobial resistance (AMR). The 2022 Global Antimicrobial Resistance and Use Surveillance System (GLASS) report indicates that, across 76 reporting countries, the median prevalence of resistance shown by *Escherichia coli* (*E. coli*) to third-generation cephalosporins was approximately 42%, reflecting widespread reduced susceptibility to this critical class of antibiotics [1]. This problem is particularly severe across healthcare, environmental, and industrial settings affected by infections caused by multidrug-resistant organisms.

E. coli is a clinically relevant model organism for studying the AMR crisis. As a Gram-negative bacterium present in the intestinal tract and a leading cause of urinary tract infections, bloodstream infections, and meningitis, it has demonstrated a strong capacity for rapid acquisition of resistance [2]. The global spread of *E. coli* strains, producing extended-spectrum β-lactamases (ESBLs) and carbapenemases, has severely compromised the effectiveness of frontline β-lactam therapies [3]. In addition to resistance mechanisms elucidated in past studies, the outer membrane of *E. coli*, with its lipopolysaccharide outer leaflet, acts as a permeability barrier restricting the entry of many antibacterial molecules [4]. Together, these intrinsic and acquired features make *E. coli* a clinically representative and in-demand model for evaluating novel antibacterial strategies.

These compounding challenges provide strong scientific and clinical motivation for the development of antibacterial approaches that operate via mechanisms distinct from those targeted by conventional antibiotics. Materials-based strategies are particularly promising in this context because such materials can act through multiple antibacterial pathways simultaneously. For example, materials that release toxic metal ions or generate reactive oxygen species (ROS) can induce membrane disruption, oxidative damage to lipids, proteins, and nucleic acids, and interference with essential cellular enzymes and metabolic processes [5–8]. A recent review also emphasized that combining metal-ion release, ROS generation, and other antibacterial mechanisms within a single material platform can enhance the antibacterial efficacy relative to single-mechanism systems [6]. This mechanistic diversity makes materials-based antibacterial platforms attractive candidates for application in controlling bacteria via pathways

Published under an exclusive license by KFUPM

that are less dependent on the conventional targets already compromised by antimicrobial resistance.

Metal-organic frameworks (MOFs) represent one of the most structurally versatile platforms for implementing this multitarget strategy. They are crystalline porous coordination polymers formed from metal-containing nodes and organic linkers assembled into one-, two-, or three-dimensional networks[7]. Key characteristics of MOFs include high porosity, large internal surface area, tunable pore size and geometry, permanent crystalline structure, and tunable metal nodes and organic linkers[8]. This structural diversity provides compositional control and characterizability that support rigorous mechanistic investigation, which is particularly important for understanding the specific contribution of individual structural parameters to antibacterial activity. Of late, there has been increased research on MOF-based antibacterial materials that can, under optimal conditions, achieve more than 90% growth inhibition against multidrug-resistant Gram-negative bacteria, supporting their potential role in next-generation infection control strategies[9].

Among the main metals investigated in this study, magnesium (Mg^{2+}) is an essential divalent cation that plays a central role in bacterial physiology. Bacteria can sense Mg^{2+} concentrations both in their environment and within the cytoplasm, allowing them to regulate Mg^{2+} transporters and other proteins that modify the cell envelope to maintain magnesium homeostasis through transporter expression, transporter activity, and cell-envelope composition; these processes are also linked to bacterial virulence[10]. One of the most important functions of Mg^{2+} is stabilizing ribosomal complexes required for protein synthesis, as intracellular Mg^{2+} helps maintain proper assembly of the 70S ribosome[11]. Increased Mg^{2+} availability can also enhance bacterial tolerance to toxic ions such as cesium (Cs^{+}), likely by preventing ribosome collapse and maintaining intracellular ion balance during metal stress[12]. Despite its essential role in bacterial physiology, magnesium-based materials corrode in aqueous environments through the reaction $Mg + 2H_2O \rightarrow Mg(OH)_2 + H_2$, releasing hydroxide ions that elevate local pH. This process has been shown to raise the surrounding pH above 10 under saline conditions, which can be harmful to bacteria[13]. However, when Mg^{2+} levels rise beyond the range that cells can effectively manage, this balance may be disturbed, and bacterial growth or biofilm-related behavior may be affected[14]. Therefore, this antibacterial effect is generally weaker at low concentrations and more condition-dependent than that of intrinsically toxic metal ions because Mg^{2+} is a biologically important ion that bacteria are already adapted to sense, transport, and utilize. Therefore, Mg-MOF-74 was used in this study as a biologically relevant parent framework and baseline comparator for evaluating the additional antibacterial contributions of Zn^{2+} and Cd^{2+} incorporation.

Zinc (Zn^{2+}) is also an essential metal in bacterial physiology, where it serves as a cofactor for numerous proteins and enzymes. To maintain zinc homeostasis, bacteria tightly regulate intracellular Zn^{2+} through uptake and efflux systems. Under zinc limitation, repression by Zur is relieved, allowing uptake systems such as ZnuABC to import more Zn^{2+}, whereas excess Zn^{2+} can lead to toxicity[15]. Zinc is also useful in antibacterial materials. When bacteria are overloaded with zinc, excess ions can disrupt gene regulation, damage key proteins, increase reactive oxygen species (ROS), and damage bacterial DNA[16]. For this reason, Zn-Mg-MOF-74 was used in this study to assess whether incorporation of Zn^{2+} into the Mg-MOF-74 framework enhances antibacterial activity relative to the Mg-only parent material.

For cadmium (Cd^{2+}), toxicity in *E. coli* is mainly attributed to its strong affinity for sulfur-containing targets, including thiol groups and sulfur species involved in cysteine and iron–sulfur cluster biosynthesis, thereby disrupting protein function and other essential cellular processes[17]. Cadmium exposure also induces oxidative-stress and damage-repair responses, indicating that it interferes with multiple bacterial functions and can therefore be exploited for antibacterial activity[18]. Thus, Cd-Mg-MOF-74 was included in this study to assess whether incorporation of Cd^{2+} into the Mg-MOF-74 framework enhances antibacterial activity relative to the Mg-only parent material.

Although a growing body of literature has demonstrated the antibacterial potential of MOF-based materials, some comparative studies were conducted to evaluate frameworks that differ in both metal-node composition and structural parameters, such as organic linker chemistry, pore geometry, and topology. These differences make it difficult to isolate the specific contribution of the metal node to antibacterial performance. In this study, the MOF-74 topology was selected as a shared parent framework to address this limitation. By maintaining the same organic linker and synthesis protocol across all three variants while varying only the metal-node composition, this study enables a controlled and direct comparison of the antibacterial contributions of Mg^{2+}, Zn^{2+}, and Cd^{2+} within the same structural context.

Therefore, this study was aimed at evaluating and comparing the antibacterial activities of Mg-MOF-74, Zn-Mg-MOF-74, and Cd-Mg-MOF-74 against *E. coli* using a broth-based OD_{600} growth inhibition assay across a concentration range of 0–2.22 mg/mL and correlating the observed responses with the metal-node chemistry of each variant. The specific objectives are: (i) to compare concentration-dependent growth inhibition profiles across all three variants under identical conditions and (ii) to correlate antibacterial performance with the known biological chemistry of Mg^{2+}, Zn^{2+}, and Cd^{2+}.

2. METHODOLOGY

This study followed an experimental design in which three MOF-74 variants were synthesized, characterized, and evaluated for antibacterial activity against *E. coli* under identical, controlled laboratory conditions. This approach enabled direct comparison among the variants while keeping other experimental variables constant, allowing observed differences in antibacterial performance to be attributed primarily to metal incorporation.

2.1. Materials and Chemicals. The following chemicals were used for MOF synthesis and were purchased from Sigma-Aldrich: magnesium nitrate hexahydrate ($Mg(NO_3)_2 \cdot 6H_2O$), zinc nitrate hexahydrate ($Zn(NO_3)_2 \cdot 6H_2O$), and cadmium nitrate tetrahydrate ($Cd(NO_3)_2 \cdot 4H_2O$) as metal precursors; 2,5-dihydroxyterephthalic acid (DHTA, 98%) as the organic linker; and N,N-dimethylformamide (DMF, anhydrous, 99.8%), ethanol, and deionized water (DI H_2O) as the solvent system.

All reagents were of analytical or reagent grade and were used as received without further purification. The products were washed three times with DMF, with centrifugation after each wash, followed by three washes with ethanol, with centrifugation between washing steps. For the antibacterial assay, Luria–Bertani (LB) broth was used as the bacterial growth medium. Additional materials included sterile 15-mL polypropylene test tubes, 1.5-mL microcentrifuge tubes, sterile pipette tips, and an analytical balance. All glassware and growth media were autoclaved before use.

2.2. Synthesis of MOF-74 Variants.

2.2.1. Synthesis of Mg-MOF-74. Mg-MOF-74 was synthesized using a solvothermal method. $Mg(NO_3)2 \cdot 6H_2O$ (0.6650 g) and DHTA (0.1550 g) were dissolved in a solvent mixture consisting of 61.8 mL DMF, 4.1 mL ethanol, and 4.1 mL deionized water. The solution was stirred until complete dissolution, transferred into an autoclave, sealed, and heated in an oven at 120 °C for 24 h. After the reaction, the autoclave was allowed to cool to room temperature. The product was recovered by filtration, washed sequentially three times with DMF and three times with ethanol, with centrifugation between each washing step to remove unreacted precursors and residual solvent, and then dried before characterization and use.

2.2.2. Synthesis of Zn-Mg-MOF-74. Zn-Mg-MOF-74 was synthesized using the same solvothermal method. $Mg(NO_3)_2 \cdot 6H_2O$ (0.3325 g) and an equimolar amount of $Zn(NO_3)_2 \cdot 6H_2O$ were dissolved with DHTA (0.1550 g) in a solvent mixture consisting of 61.8 mL DMF, 4.1 mL absolute ethanol, and 4.1 mL deionized water. The solution was stirred until complete dissolution, transferred into an autoclave, sealed, and heated in an oven at 120 °C for 24 h. After the reaction, the autoclave was allowed to cool to room temperature. The product was recovered by filtration, washed sequentially three times with DMF and three times with ethanol, with centrifugation between each washing step to remove unreacted precursors and residual solvent, and then dried before characterization and use.

2.2.3. Synthesis of Cd-Mg-MOF-74. Cd-Mg-MOF-74 was synthesized using the same solvothermal method. $Mg(NO_3)_2 \cdot 6H_2O$ (0.3325 g) and an equimolar amount of $Cd(NO_3)_2 \cdot 4H_2O$ were dissolved with DHTA (0.1550 g) in a solvent mixture consisting of 61.8 mL DMF, 4.1 mL absolute ethanol, and 4.1 mL deionized water. The solution was stirred until complete dissolution, transferred into an autoclave, sealed, and heated in an oven at 120 °C for 24 h. After the reaction, the autoclave was allowed to cool to room temperature. The product was recovered by filtration, washed sequentially with DMF and ethanol to remove unreacted precursors and residual solvent, and then dried before characterization and use.

2.3. Characterization.

2.3.1. Powder x-ray diffraction (PXRD). PXRD analysis was performed to evaluate the structural characteristics of the synthesized materials and to confirm formation of the expected MOF-74-type framework. The measured patterns were compared against a simulated Mg-MOF-74 reference pattern generated from the crystallographic information file (CIF) obtained from the Cambridge Crystallographic Data Centre (CCDC; deposition number 1863524).

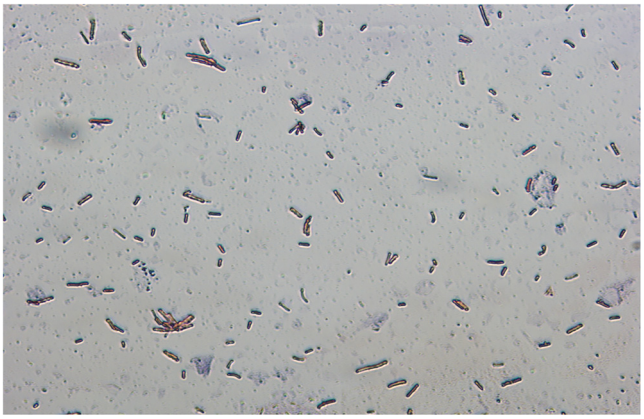

Figure 1. Optical microscopy image of *Escherichia coli* cells used in the antibacterial assays

2.3.2. Scanning electron microscopy and energy-dispersive x-ray spectroscopy (SEM/EDX). Scanning electron microscopy (SEM) was used to examine the morphology of the synthesized MOF-74 variants, whereas energy-dispersive X-ray spectroscopy (EDX) was used to confirm their elemental composition.

2.4. Bacterial Culture Preparation. *Escherichia coli* (ATCC 25922) was selected as the test organism because it is one of the most clinically significant and thoroughly characterized Gram-negative pathogens. Its outer membrane permeability barrier makes it a stringent and representative model for evaluating materials-based antibacterial agents, and its well-characterized, reproducible growth kinetics in LB medium make it suitable for quantitative growth assays [2].

Working cultures were prepared from frozen glycerol stocks by streaking onto LB agar plates and incubating overnight at 37 °C to obtain isolated colonies. A single isolated colony was used to inoculate 10 mL of LB broth in a sterile 50-mL Erlenmeyer flask, which was then incubated overnight at 37 °C with orbital shaking at 200 rpm to produce a stationary-phase culture. Before each experiment, this overnight culture was diluted in fresh LB broth and incubated for an additional 2–3 h at 37 °C with orbital shaking to obtain a mid-exponential-phase culture. OD_{600} was measured using a JASCO V-760 UV–Vis spectrophotometer and used to prepare standardized bacterial suspensions at approximately 10^6 colony-forming units (CFU)/mL in fresh LB broth. The rod-shaped morphology of the *E. coli* culture used in this study was confirmed by optical microscopy before the antibacterial assay, as shown in Figure 1, and was consistent with the characteristic bacillary morphology of this organism.

2.5. Antibacterial Exposure Assay. For each MOF-74 variant, the appropriate mass of dry MOF powder was weighed on an analytical balance and dispersed in LB broth by vortexing for 10 s immediately before addition to bacterial cultures. Each variant was tested at final concentrations of 0, 0.11, 0.56, 1.11, 1.67, and 2.22 mg/mL. An untreated positive control containing bacteria in LB broth without MOF was included in each experiment. All conditions were performed in duplicate (n = 2), and

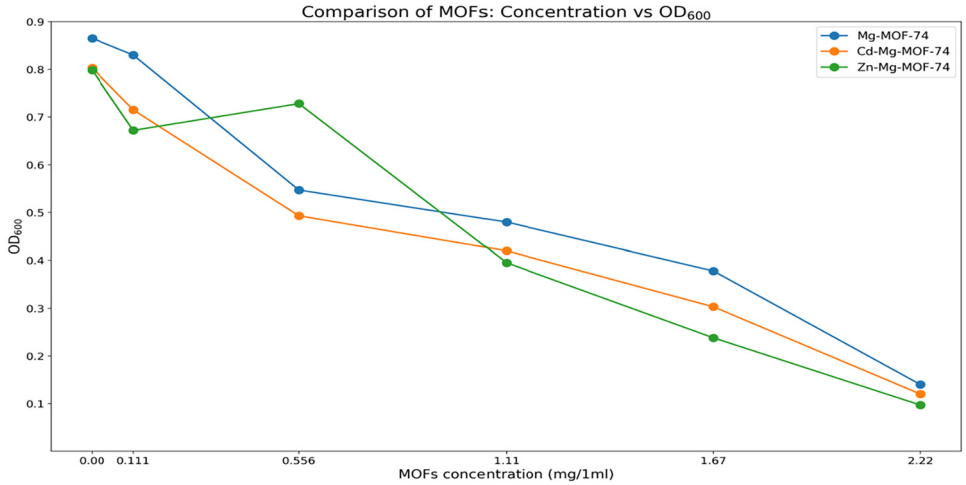

Figure 2. Comparative plot of concentration-dependent OD_{600} responses of *E. coli* cultures treated with Mg-MOF-74, Cd-Mg-MOF-74, and Zn-Mg-MOF-74 over 24 h at concentrations of 0-2.22 mg/mL

the average values were used in the Results section. Cultures were incubated at 37 °C for 24 h with continuous orbital shaking at 200 rpm to maintain aerobic conditions and ensure uniform MOF particle distribution throughout the culture.

After 24 h, cultures were briefly vortexed, and optical density at 600 nm (OD_{600}) was measured using a JASCO V-760 UV–Vis spectrophotometer calibrated at 600 nm. Visual turbidity assessment of all cultures was also performed under consistent lighting conditions.

2.6. Growth Inhibition Calculation and Statistical Analysis. OD_{600} values were used to calculate percentage growth inhibition (GI%) relative to the untreated positive control using the following equation:

$$GI\% = [(OD_{600}\ \text{control} - OD_{600}\ \text{treated})/OD_{600}\ \text{control}] \times 100$$

As all conditions were performed in duplicate ($n = 2$), results are reported as mean OD_{600} values; formal inferential statistical analysis was not performed. Results were presented as concentration–response profiles plotting OD_{600} and GI% against MOF concentration for each variant.

3. RESULTS AND DISCUSSION

3.1. Structural and Compositional Characterization. The PXRD patterns of the three synthesized variants are shown in Figure 3. All three variants exhibited characteristic low-angle reflections near $2\theta \approx 6.8°$ and $2\theta \approx 11.7°–12°$, which are consistent with previously reported diffraction patterns for MOF-74-type structures. The simulated Mg-MOF-74 reference pattern (CCDC deposition number 1863524) was used for comparison and further supports the formation of MOF-74-type frameworks in the synthesized samples.

The Mg-MOF-74 sample displayed two clear low-angle reflections that closely matched the simulated pattern, indicating successful formation of the Mg-based MOF-74 framework with reasonable crystallinity. Zn-Mg-MOF-74 also exhibited reflections characteristic of the MOF-74 topology; however, the peaks appeared broader and less sharply resolved than those observed for the Cd-containing variant. This may indicate slightly reduced crystalline order, as peak broadening in X-ray diffraction patterns is commonly associated with reduced crystallite size or lattice defects [19].

Overall, the PXRD results indicate that all synthesized materials retained the characteristic MOF-74-type structure while exhibiting differences in crystallinity and peak sharpness associated with variations in metal-node composition. Differences in crystalline order among the variants do not necessarily compromise the validity of the antibacterial comparison, as functional antibacterial activity in MOF-based systems is not strictly dependent on high crystallinity and can arise from metal-ion release and surface interactions regardless of the degree of crystallinity.

Scanning electron microscopy (SEM) and energy-dispersive X-ray spectroscopy (EDX) were used to examine the morphology and elemental composition of the three variants, as shown in Figure 4. SEM imaging revealed noticeable morphological differences among the three variants. Mg-MOF-74 exhibited relatively

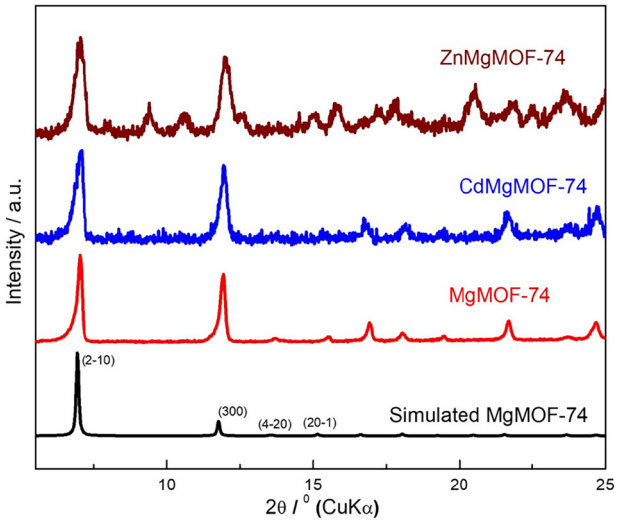

Figure 3. Powder X-ray diffraction (PXRD) patterns of Cd-Mg-MOF-74, Zn-Mg-MOF-74, and Mg-MOF-74

Table 1. *OD_{600} values and calculated growth inhibition (GI%) for each MOF-74 variant at each tested concentration against E. coli after 24 h*

Concentration (mg/1 mL)	Mg-MOF-74 OD_{600}	Mg GI%	Cd-Mg-MOF-74 OD_{600}	Cd GI%	Zn-Mg-MOF-74 OD_{600}	Zn GI%
0.0000 (control)	0.8653 range (0.8649-0.8657)	—	0.8046 range (0.8032-0.8060)	—	0.8005 range (0.8001-0.8010)	—
0.1111	0.8316 range (0.8311-0.8321)	3.9%	0.7149 range (0.7143-0.7155)	11.1%	0.6695 range (0.6692-0.6699)	16.4%
0.5556	0.5471 range (0.5469-0.5474)	36.8%	0.4940 range (0.4925-0.4955)	38.6%	0.7280 range (0.7270-0.7290)	9.1%
1.1111	0.4790 range (0.4781-0.4799)	44.6%	0.4176 range (0.4171-0.4181)	48.1%	0.3944 range (0.3942-0.3946)	50.7%
1.6667	0.3760 range (0.3752-0.3768)	56.5%	0.3010 range (0.2991-0.3029)	62.6%	0.2375 range (0.2366-0.2385)	70.3%
2.2222	0.1394 range (0.1393-0.1395)	83.9%	0.1169 range (0.1165-0.1174)	85.5%	0.0955 range (0.0946-0.0965)	88.1%

large leaf- to petal-shaped particles that formed loosely stacked aggregates. In contrast, Zn-Mg-MOF-74 displayed considerably smaller, more irregular, blocky particles that were densely aggregated, suggesting that incorporation of Zn^{2+} influenced particle formation and morphology. Cd-Mg-MOF-74 showed intermediate morphology, consisting of larger platelet-like particles similar to Mg-MOF-74, along with regions of smaller aggregated particles. Overall, these observations suggest that incorporation of Zn^{2+} and Cd^{2+} affects particle size, shape, and aggregation behavior.

EDX analysis was performed on all three MOF-74 variants to confirm their elemental composition, and the results are presented alongside the SEM images in Figure 2 and Table 1. For Mg-MOF-74, characteristic peaks corresponding to C, O, and Mg were detected, with Mg accounting for 14.68 wt% (9.17 at%). No additional metal peaks were observed, indicating the absence of secondary metal components in the parent material. For Zn-Mg-MOF-74, distinct Zn peaks were detected at approximately 8.6 and 9.6 keV in addition to the expected C, O, and Mg signals. Semi-quantitative analysis yielded 6.69 wt% Mg (4.42 at%) and 13.71 wt% Zn (3.37 at%), corresponding to an Mg:Zn atomic ratio of approximately 1.3:1. These results confirm that Zn^{2+} was successfully incorporated into the framework alongside Mg^{2+}. For Cd-Mg-MOF-74, distinct Cd peaks were detected at approximately 3.1 and 3.3 keV alongside the Mg, C, and O signals. Semi-quantitative analysis yielded 10.10 wt% Mg (8.00 at%) and 25.30 wt% Cd (4.33 at%), corresponding to an Mg:Cd atomic ratio of approximately 1.9:1. This indicates that magnesium remained the dominant metal component, with Cd^{2+} incorporated as a secondary metal component. Taken together, these EDX results confirm the successful incorporation of both Zn^{2+} and Cd^{2+} into the Mg-MOF-74 framework and provide direct compositional evidence for the formation of bimetallic MOF-74 variants. Although EDX provides semi-quantitative elemental information, more precise determination of metal stoichiometry would require inductively coupled plasma (ICP) analysis, which is recommended for future research.

The antibacterial activity of all three MOF-74 variants against *E. coli* was assessed by measuring OD_{600} after 24 h of exposure across concentrations of 0-2.22 mg/mL. The OD_{600} values and calculated growth inhibition (GI%) for each variant are summarized in Table 1, and the concentration-response profiles are shown in Figure 2.

3.2. Antibacterial Activity of Mg-MOF-74. Treatment of *E. coli* cultures with Mg-MOF-74 across the concentration range of 0-2.22 mg/mL produced a gradual, concentration-dependent decrease in OD_{600}, as shown in Figure 4. In the comparison plot, the Mg-MOF-74 curve remained above both bimetallic variants across most of the concentration range, reflecting its weaker inhibitory effect relative to Cd-Mg-MOF-74 and Zn-Mg-MOF-74 at equivalent concentrations.

At the lowest tested concentration of 0.11 mg/mL, growth inhibition was very low, with an OD_{600} of 0.8316 (GI% = 3.9%), which was nearly indistinguishable from the untreated control. This negligible early activity is consistent with the known physiology of Mg^{2+} in bacteria, as *E. coli* possesses multiple mechanisms that enable cells to sense elevated extracellular Mg^{2+} and respond by adjusting ion uptake and efflux, allowing broad tolerance of Mg^{2+} concentrations without substantial growth disruption [10]. As a result, low doses of Mg-MOF-74 may be insufficient to overwhelm these homeostatic mechanisms, and the framework exerts only marginal inhibitory effects at early concentration points.

As concentration increased, OD_{600} declined progressively: 0.5471 (GI% = 36.8%) at 0.56 mg/mL, 0.4790 (GI% = 44.6%) at 1.11 mg/mL, and 0.3760 (GI% = 56.5%) at 1.67 mg/mL. At the highest tested concentration of 2.22 mg/mL, OD_{600} decreased to 0.1394 (GI% = 83.9%). This stronger inhibition at elevated particle loads relative to lower concentrations is likely explained by two contributing factors. First, the high particle load in a small volume of broth may introduce physical effects, such as direct contact between the dense MOF suspension and bacterial cells and reduced nutrient availability in the medium, both of which scale with concentration regardless of metal-node identity. Second, at sufficiently high external Mg^{2+} concentrations, the capacity of bacterial homeostatic systems, such as CorA and MgtA, to regulate intracellular Mg^{2+} levels may be exceeded, disrupting cellular balance and further contributing to growth inhibition. Although these two mechanisms cannot be separated using the current dataset, both are consistent with the concentration-dependent profile observed for Mg-MOF-74 and

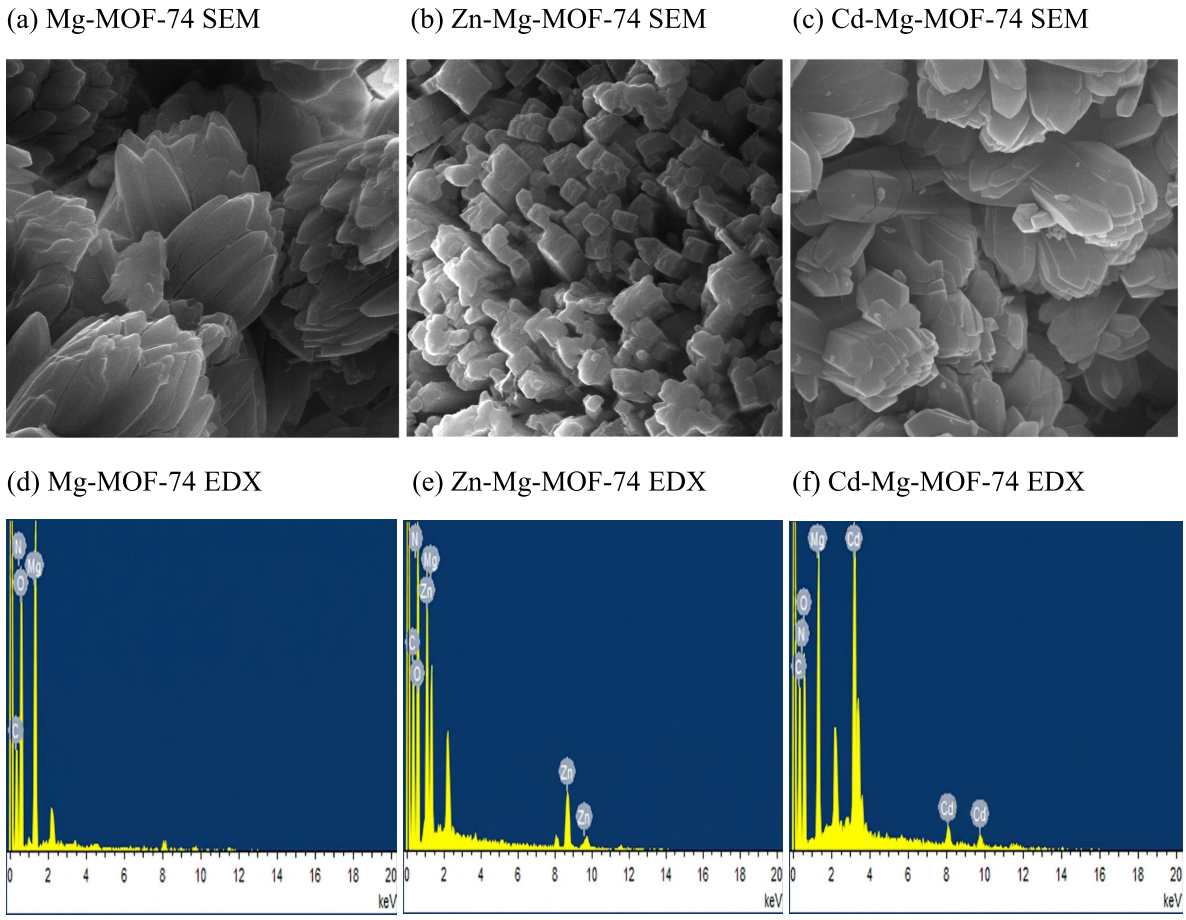

Figure 4. SEM images and EDX spectra of synthesized MOF-74 variants: (a) Mg-MOF-74 SEM, (b) Zn-Mg-MOF-74 SEM, (c) Cd-Mg-MOF-74 SEM, (d) Mg-MOF-74 EDX spectrum, (e) Zn-Mg-MOF-74 EDX spectrum, and (f) Cd-Mg-MOF-74 EDX spectrum

explain why inhibition increases more steeply at higher particle loads despite the limited intrinsic toxicity of Mg^{2+} at low concentrations.

Mg-based materials can also elevate local pH through the release of hydroxide ions, a process that has been shown to raise the surrounding pH above 10 under saline conditions.[13] This pH elevation may contribute to the observed growth inhibition of Mg-MOF-74, particularly at higher concentrations where greater material dissolution is expected. However, broth pH was not measured in this study. As a result, the relative contribution of pH-mediated effects versus direct Mg^{2+} ion interactions cannot be distinguished from the current dataset, and this remains an important consideration for future mechanistic investigation.

3.3. Antibacterial Activity of Zn-Mg-MOF-74. Zn-Mg-MOF-74 displayed a notable response pattern at low concentrations, as shown by the green curve in Figure 4. At 0.11 mg/mL, OD_{600} was 0.6695, corresponding to the highest early-onset inhibition among all variants at this concentration (GI% = 16.4%); at this point, green curve was noticeably lower than both other variants. However, OD_{600} increased to 0.7280 at 0.56 mg/mL (GI% = 9.1%), producing the upward deviation observed in the green curve between 0.11 and 0.56 mg/mL in Figure 4. This increase placed the Zn-containing variant above the Cd-containing variant and close to the Mg-only variant at 0.56 mg/mL. The deviation may reflect experimental variability at this concentration or a transient bacterial adaptive response to sub-lethal zinc exposure.

From 1.11 mg/mL onward, the green curve decreased sharply and remained below both other variants, as shown in Figure 4. OD_{600} decreased to 0.3944 (GI% = 50.7%) at 1.11 mg/mL and

Table 2. *Semi-quantitative EDX elemental composition of synthesized MOF-74 variants*

Sample	Element	Weight %	Atomic %
Mg-MOF-74	C	30.35	38.37
	O	52.87	50.19
	Mg	14.68	9.17
Zn-Mg-MOF-74	C	37.42	49.98
	O	42.63	42.75
	Mg	6.69	4.42
	Zn	13.71	3.37
Cd-Mg-MOF-74	C	24.93	39.94
	O	39.67	47.72
	Mg	10.10	8.00
	Cd	25.30	4.33

0.2375 (GI% = 70.3%) at 1.67 mg/mL. At 2.22 mg/mL, Zn-Mg-MOF-74 reached the lowest terminal OD_{600} among all three variants, with an OD_{600} of 0.0955 (GI% = 88.1%).

The antibacterial activity of Zn-Mg-MOF-74 is mechanistically consistent with the established biological effects of excess Zn^{2+} in bacterial systems. Under physiological conditions, bacteria maintain intracellular Zn^{2+} homeostasis through tightly regulated uptake and efflux systems, including regulatory networks such as Zur and transport systems such as ZnuABC[15]. When Zn^{2+} levels exceed the capacity of these homeostatic mechanisms, zinc overloading can occur, leading to disruption of bacterial transcriptional control, inactivation of functional proteins, generation of intracellular reactive oxygen species (ROS), and damage to bacterial DNA[16]. These multifaceted toxic effects provide a mechanistic basis for the concentration-dependent growth inhibition observed for Zn-Mg-MOF-74, particularly at lower concentrations, where metal-specific biochemical interactions are expected to play a larger role than non-specific particle-mediated effects. At reduced particle loadings, physical crowding and contact-based interactions are limited, while Zn^{2+}-mediated biochemical toxicity may still occur.

Overall, this ROS-associated mechanism is consistent with the established antibacterial activity of Zn^{2+}, in which oxidative stress contributes substantially to bacterial inhibition.

3.4. Antibacterial Activity of Cd-Mg-MOF-74. Cd-Mg-MOF-74 produced the most consistent concentration–response profile of the three variants, shown as the orange curve in Figure 4. The curve decreased steadily across the full concentration range from 0 to 2.22 mg/mL without the deviation observed for the Zn-containing variant. At the lowest tested concentration of 0.11 mg/mL, OD_{600} was 0.7149 (GI% = 11.1%), placing the orange curve between the blue Mg curve and the green Zn curve. This result reflects greater early inhibition than that produced by the Mg-only framework but slightly lower inhibition than that produced by the Zn-containing variant. These findings suggest that Cd incorporation improved antibacterial activity relative to the Mg-only framework, although its early inhibition remained slightly weaker than that of the Zn-containing variant. At 0.56 mg/mL, the orange curve decreased more substantially than the green curve, reaching OD_{600} = 0.4940 (GI% = 38.6%). From this concentration onward, the Cd and Zn curves remained relatively close until 1.67 mg/mL, as shown in Figure 2.

Inhibition continued to increase steadily, with OD_{600} = 0.4176 (GI% = 48.1%) at 1.11 mg/mL and OD_{600} = 0.3010 (GI% = 62.6%) at 1.67 mg/mL. At 2.22 mg/mL, the orange curve converged with the green curve at the lower end of Figure 4, reaching OD_{600} = 0.1169 (GI% = 85.5%).

The decreasing profile of Cd-Mg-MOF-74 is mechanistically consistent with the toxicity of Cd^{2+} in *E. coli* across the tested range. Cd^{2+} can disrupt bacterial protein function through interactions with thiol-containing biomolecules and can interfere with essential cellular processes[17,18]. Overall, Cd-Mg-MOF-74 demonstrated strong and consistent antibacterial activity, although its terminal performance remained slightly lower than that of Zn-Mg-MOF-74.

3.5. Comparative Summary. As shown in Figure 2, all three variants produced concentration-dependent reductions in OD_{600} over the range of 0-2.22 mg/mL, and all three curves converged toward a similar inhibitory plateau at the highest tested concentration. The three curves were most clearly separated in two regions: at 0.11 mg/mL, where the green Zn curve was lowest, followed by the orange Cd curve and then the blue Mg curve; and between 1.11 and 1.67 mg/mL, where the green and orange curves both remained clearly below the blue curve. These trends demonstrate that the bimetallic variants outperformed the Mg-only control in the low-to-intermediate concentration range.

The overall performance hierarchy at 2.22 mg/mL was Zn-Mg-MOF-74 (GI% = 88.1%) >Cd-Mg-MOF-74 (GI% = 85.5%) >Mg-MOF-74 (GI% = 83.9%). However, the narrow separation among all three curves at this concentration suggests that the differences observed at 2.22 mg/mL may be attributable to non-specific, concentration-driven effects shared by all variants, such as physical crowding of bacterial cells and reduced nutrient availability in a dense particle suspension, rather than to metal-node-specific toxicity mechanisms. This interpretation cannot be confirmed without further investigation. Consequently, the most mechanistically informative evidence for metal-node-driven antibacterial activity occurs at low concentrations, particularly at 0.11 mg/mL, where the bimetallic variants exhibited clearly superior inhibition relative to Mg-MOF-74 despite sharing the same organic scaffold and linker chemistry. This concentration region most clearly isolates the probable contribution of Zn^{2+} and Cd^{2+} incorporation to antibacterial performance and therefore provides the strongest basis for suggesting that bimetallic substitution enhances the antibacterial potency of the MOF-74 framework.

The concentration-dependent inhibition trends observed in this study likely arise from a combination of metal-ion-mediated toxicity and particle-related effects. At lower concentrations, the enhanced performance of Zn-Mg-MOF-74 and Cd-Mg-MOF-74 relative to Mg-MOF-74 is consistent with ion-specific biochemical interactions. At higher concentrations, however, non-specific effects such as increased particle density and enhanced physical contact between MOF particles and bacterial cells may contribute more substantially to growth inhibition. The terminal growth inhibition achieved by all three variants (83.9–88.1% at 2.22 mg/mL) is broadly consistent with values reported for other MOF-based antibacterial materials, which have been shown to achieve more than 90% growth inhibition against Gram-negative bacteria under optimized conditions[9]. The somewhat lower inhibition observed here may reflect differences in tested concentration, bacterial strain, and assay format, and indicates that further optimization of dose and metal-node composition could enhance the antibacterial performance of the MOF-74 system.

While time-resolved ion release measurements were not performed in this study, the observed differences between the bimetallic and Mg-only variants at low concentrations suggest that metal-node chemistry plays a key role in antibacterial performance, independent of purely physical particle effects.

4. CONCLUSION

This study evaluated and compared the antibacterial activity of three MOF-74 variants (Mg-MOF-74, Zn-Mg-MOF-74, and Cd-Mg-MOF-74) against *Escherichia coli* using an OD_{600}-based

growth inhibition assay. The results demonstrated an interpretable performance hierarchy: Zn-Mg-MOF-74 exhibited the strongest antibacterial activity, followed by Cd-Mg-MOF-74, while Mg-MOF-74 produced comparatively lower growth inhibition at lower concentrations, likely reflecting the relatively lower intrinsic antibacterial potency of Mg^{2+} compared to Zn^{2+} and Cd^{2+}; notably, Mg-MOF-74 still achieved substantial inhibition (83.9%) at the highest tested concentration, indicating that magnesium-based effects become clearly toxic at higher doses.

These results should be interpreted in light of certain limitations. All growth inhibition measurements were performed in duplicate ($n = 2$) rather than with a larger number of biological replicates, so the differences observed between concentrations and variants should be considered preliminary rather than statistically confirmed. In addition, the untreated control OD_{600} values differed slightly among the three assays (0.8653, 0.8046, and 0.8005), reflecting the use of independently grown bacterial cultures for each variant; because growth inhibition (GI%) was calculated relative to the matched control within each assay, this does not affect the validity of within-assay comparisons, but it does limit direct comparison of absolute OD_{600} values across variants and reinforces the value of using GI% as the primary basis for comparison.

These findings demonstrate that bimetallic MOF-74 variants incorporating Zn^{2+} or Cd^{2+} with the Mg-MOF-74 scaffold retain strong antibacterial activity, suggesting that mixed-metal strategies can be employed to tune antibacterial potency. More broadly, bimetallic MOF-74 variants represent a structurally defined, compositionally tunable platform for the rational design of next-generation antibacterial materials, offering a potential route toward addressing the growing challenge of antimicrobial resistance.

Future work should include quantitative measurement of Mg^{2+}, Zn^{2+}, and Cd^{2+} ion release under antibacterial assay conditions, pH monitoring throughout bacterial exposure, and cytotoxicity evaluation against mammalian cell lines, particularly for the Cd-containing variant. Evaluation against clinical *E. coli* isolates, including ESBL-producing and carbapenem-resistant strains, would also be necessary to assess the translational relevance of the findings beyond the laboratory strain used in the present study.

In addition, expanding the investigation to include different Zn:Mg and Cd:Mg ratios, as well as additional bimetallic combinations within the MOF-74 family, would provide broader insight into how metal-node engineering influences antibacterial performance. Furthermore, encapsulation of antibacterial agents such as antimicrobial peptides, antibiotics, or photosensitizers within the porous MOF-74 framework represents a promising strategy for developing multifunctional platforms that combine metal-ion-mediated toxicity with drug delivery, potentially enhancing efficacy against drug-resistant organisms.

AFFILIATIONS AND AUTHOR DETAILS

Undergraduate Author

Omar Buqes – *Bioengineering Department, King Fahd University of Petroleum & Minerals, Dhahran 31261, Saudi Arabia*;
Email: bogisomar@gmail.com

Corresponding Author

Amjad Khalil – *Research Mentor, Bioengineering Department, King Fahd University of Petroleum & Minerals, Dhahran 31261, Saudi Arabia*;
Email: amjadb@kfupm.edu.sa

Aasif Helal – *Research Mentor, Interdisciplinary Research Center for Hydrogen Technologies and Carbon Management IRC (IRC-HTCM), King Fahd University of Petroleum & Minerals, Dhahran 31261, Saudi Arabia*;
Email: alsharafi@kfupm.edu.sa

ACKNOWLEDGEMENTS

The authors acknowledge the Department of BioEngineering at King Fahd University of Petroleum & Minerals (KFUPM) for providing access to the laboratory facilities and instrumentation used in this study.

REFERENCES

(1) World Health Organization. *Global Antimicrobial Resistance and Use Surveillance System (GLASS) Report 2022*. World Health Organization (2022).

(2) Kaper, J. B., Nataro, J. P. & Mobley, H. L. T. Pathogenic *Escherichia coli*. *Nat. Rev. Microbiol.* **2**, 123–140 (2004).

(3) Poirel, L., Madec, J.-Y., Lupo, A., Schink, A.-K., Kieffer, N., Nordmann, P. & Schwarz, S. Antimicrobial resistance in *Escherichia coli*. *Microbiol. Spectr.* **6**, ARBA-0026-2017 (2018).

(4) Ghai, I. A barrier to entry: examining the bacterial outer membrane and antibiotic resistance. *Appl. Sci.* **13**, 4238 (2023).

(5) Tian, Y., Wang, B., Zhang, Z., Kai, T., Wu, P. & Ding, P. Recent advances in metal–organic frameworks for antibacterial applications: mechanisms and emerging strategies. *RSC Adv.* **15**, 26710–26727 (2025).

(6) Generalova, A. N. & Dushina, A. O. Metal/metal oxide nanoparticles with antibacterial activity and their potential to disrupt bacterial biofilms: recent advances with emphasis on the underlying mechanisms. *Adv. Colloid Interface Sci.* **345**, 103626 (2025).

(7) Saif, M. S., Batool, S., Majeed, Y., Asadullah, Tariq, T., Haitao, L., Duan, Y., Mustafa, G. & Hasan, M. Metal–organic frameworks (MOFs) synthesis and their use as a loading agent in oxidative stress-based diseases. *J. Environ. Chem. Eng.* **13**, 118725 (2025).

(8) Raptopoulou, C. P. Metal–organic frameworks: synthetic methods and potential applications. *Materials* **14**, 310 (2021).

(9) Hubab, M. & Al-Ghouti, M. A. Recent advances and potential applications for metal–organic frameworks (MOFs) and MOFs-derived materials: characterizations and antimicrobial activities. *Biotechnol. Rep.* **42**, e00837 (2024).

(10) Groisman, E. A., Hollands, K., Kriner, M. A., Lee, E. J., Park, S. Y. & Pontes, M. H. Bacterial Mg^{2+} homeostasis, transport, and virulence. *Annu. Rev. Genet.* **47**, 625–646 (2013).

(11) Akanuma, G., Yamazaki, K., Yagishi, Y., Iizuka, Y., Ishizuka, M., Kawamura, F. & Kato-Yamada, Y. Magnesium suppresses defects in the formation of 70S ribosomes as well as in sporulation caused by lack of several individual ribosomal proteins. *J. Bacteriol.* **200**, e00212-18 (2018).

(12) Ishida, Y., Zhang, C., Satoh, K. & Ito, M. Physiological importance and role of Mg^{2+} in improving bacterial resistance to cesium. *Front. Microbiol.* **14**, 1201121 (2023).

(13) Song, Q., Yang, L., Yi, F., Chen, C., Guo, J., Qi, Z. & Song, Y. Antibacterial pure magnesium and magnesium alloys for biomedical materials—a review. *Crystals* **14**, 939 (2024).

(14) Demishtein, K., Reifen, R. & Shemesh, M. Antimicrobial properties of magnesium open opportunities to develop healthier food. *Nutrients* **11**, 2363 (2019).

(15) Hussain, S., Khan, M., Sheikh, T. M. M., Mumtaz, M. Z., Chohan, T. A., Shamim, S. & Liu, Y. Zinc essentiality, toxicity, and its bacterial bioremediation: a comprehensive insight. *Front. Microbiol.* **13**, 900740 (2022).

(16) De Rose, D. U., Mirotta, N., Dotta, A., Salvatori, G., Ronchetti, M. P., Campogiani, L., Ceccherini-Silberstein, F. & Iannetta, M. The role of zinc against bacterial infections in neonates, children, and adults: a scoping review from the available evidence of randomized controlled trials about zinc supplementation to new research opportunities. *Antibiotics* **15**, 66 (2026).

(17) Helbig, K., Grosse, C. & Nies, D. H. Cadmium toxicity in glutathione mutants of *Escherichia coli*. *J. Bacteriol.* **190**, 5439–5454 (2008).

(18) Davidova, S., Milushev, V. & Satchanska, G. The mechanisms of cadmium toxicity in living organisms. *Toxics* **12**, 875 (2024).

(19) Ungár, T. Microstructural parameters from X-ray diffraction peak broadening. *Scr. Mater.* **51**, 777–781 (2004).